Non-Fermi liquid behavior and quantum criticality in cubic heavy fermion systems with non-Kramers multipolar local moments

SangEun Han [*] and Daniel J. Schultz [*]
Department of Physics, University of Toronto, Toronto, Ontario M5S 1A7, Canada

Yong Baek Kim
Department of Physics, University of Toronto, Toronto, Ontario M5S 1A7, Canada
and School of Physics, Korea Institute for Advanced Study, Seoul 02455, Korea

Notable non-Fermi liquid and quantum critical behaviors are observed in rare-earth metallic systems with non-Kramers local moments supporting a number of different multipolar moments. A prominent example is Pr(Ti, V)$_2$Al$_{20}$, where the non-Kramers doublet of the Pr^{3+} ion allows quadrupolar and octupolar moments, but lacks a dipolar moment. Previous theoretical studies show that a single impurity Kondo problem with such an unusual local moment leads to exotic non-Fermi liquid states. In this work, we investigate possible quantum critical behaviors arising from the competition between non-Fermi liquid states and multipolar-ordered phases induced by the RKKY interaction. We consider a local version of the corresponding Kondo lattice model, namely the Bose-Fermi Kondo model. Here, the multipolar local moments are coupled to fermionic and bosonic bath degrees of freedom representing the multipolar Kondo effect and RKKY interactions. Using a perturbative renormalization group (RG) study up to two loop order, we find critical points between non-Fermi liquid Kondo fixed points and a quadrupolar ordered fixed point. The critical points describe quantum critical behaviors at the corresponding phase transitions and can be distinguished by higher order corrections in the octupolar susceptibility that can be measured by ultrasound experiments. Our results imply the existence of a rich expansion of the phases and quantum critical behaviors in multipolar heavy fermion systems.

I. INTRODUCTION

Due to strong spin-orbit coupling and crystal electric field effects, f electrons in rare-earth metallic systems may form higher-rank multipolar moments [1,2]. Recent studies on the relevant materials have shown that the interplay between the multipolar moments and itinerant conduction electrons can lead to a variety of exotic quantum phases of matter including multipolar ordered phases, strange metallic behavior, and unconventional superconductivity [3–18]; this interplay also provides a setting for quantum critical behavior [19–21]. In contrast to the archetypal heavy fermion systems with dipolar local moments [22,23], such materials are described by a multipolar Kondo lattice model, with the Kondo interactions and subsequent RKKY interactions taking very unusual forms [24–26]. The Pr-based caged cubic compounds Pr(Ti, V)$_2$Al$_{20}$ are a particularly exciting realization of a multipolar Kondo lattice. In this class of materials, the Pr^{3+} ions rest at the center of a tetrahedral cage, and contribute a local $4f^2$ moment. The moment forms a non-Kramers doublet in the presence of the crystal field, and lacks any dipolar moment; instead it only carries quadrupolar and octupolar moments. These moments provide a route a number of experimentally observed phenomena including a quadrupolar ordered phase, a multipolar Kondo effect related to non-Fermi

liquid behavior (with resistivity $\rho \sim T^{1/2}$ for the case of PrV$_2$Al$_{20}$), and the multipolar fluctuations responsible for the unconventional superconducting phase [27–45].

Theoretical works to understand these different quantum phases have either focused on the properties deep inside of a phase [46–54], or have been Ginzburg-Landau studies of magnetic ordering phase transitions [55]. However, a full understanding of the quantum critical behavior which may arise due to the competition between multipolar RKKY fluctuations and the Kondo effect remains elusive. A simplified approach to this competition is the Bose-Fermi Kondo model, which serves as a local approximation of the full Kondo lattice [56–65]. Within this scheme, the Kondo coupling between the local moment and conduction electrons is taken into account explicitly, but the RKKY interaction is replaced by a dynamical bosonic bath with the density of states $\sim |\omega|^{1-\epsilon}$ acting at the impurity site. The main two kinds of phases admitted by renormalization group analyses of this model are a Kondo phase with large Fermi surface, wherein the local moments hybridize with the conduction electrons increasing the total density, and a magnetically ordered phase where the Kondo effect is destroyed and the conduction electrons are decoupled from the local moments [66–70]. The latter phase is to be contrasted against the Moriya-Hertz-Millis type (potentially multipolar) spin density wave instability of a heavy Fermi liquid [71]. Although other Bose-Fermi Kondo models studied with extended dynamical mean field theory may yield a spin-density wave type phase [59,72,73], the

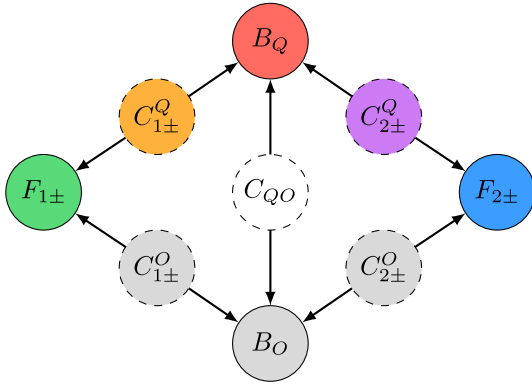*These authors contributed equally to this work.

FIG. 1. Schematic diagram for quantum phase transitions between non-Fermi liquid phases and multipolar ordered phases. $F_{1\pm}$ and $F_{2\pm}$ stand for the novel multipolar and 2-channel Kondo fixed points, respectively. B_Q and B_O stand for the quadrupolar and octupolar ordered fixed points, respectively, and C_{QO} is a critical point between B_Q and B_O. $C_{1\pm}^{Q(O)}$ and $C_{2\pm}^{Q(O)}$ are critical points between $F_{1\pm}$ and $B_{Q(O)}$, and $F_{2\pm}$ and $B_{Q(O)}$, respectively. Critical points have dashed lines, and stable fixed points have solid lines; gray circles are outside of the perturbative regime. The fixed point values are listed in Table I.

results we will describe here fall into the Kondo destruction category.

In this work, motivated by experiments on Pr-based heavy fermion systems, $Pr(Ti, V)_2Al_20$, we consider the multipolar Bose-Fermi Kondo model in cubic systems as a simplified model for the multipolar Kondo lattice. Here, the Pr^{3+} ions provide a non-Kramers doublet supporting quadrupolar and octupolar moments, which couple to conduction electrons. As shown below, the multipolar Kondo lattice model permits a mapping to a multipolar Bose-Fermi Kondo model, which can be constructed based on local point group symmetry. The fermionic Kondo problem without the bosonic bath or

RKKY interaction was theoretically studied earlier and various non-Fermi liquid ground states were identified. These results may have some relevance to experiments in the dilute limit [46,47,74–76], where non-Fermi liquid behaviors were observed. It is then natural to study the phase transition between such non-Fermi liquids and a multipolar ordered phase.

In the multipolar Bose-Fermi Kondo model, we set the density of states of the quadrupolar (Q) and octupolar (O) bosonic baths to be $|\omega|^{1-\epsilon_i}(i = Q, O)$ and perform a perturbative renormalization group (RG) analysis based on an ϵ-expansion to order ϵ^2 to study the zero temperature phase diagram of the model. Similar to previous work, we find that there are two non-Fermi liquid phases [47,54] in the fermion Kondo part of the model; one is a two-channel Kondo non-Fermi liquid, and the other is an exotic non-Fermi liquid phase, not simply classifiable into any multichannel-type model. These phases, upon tuning the Kondo and bosonic bath couplings, can pass through quantum critical points to both arrive at a quadrupolar ordered phase, as presented in the schematic diagram (Fig. 1) and in the RG flow diagrams (Figs. 2 and 3). The transition from the non-Fermi liquid phases to the quadrupolar ordered phase is accompanied by the destruction of the Kondo effect such that the Kondo coupling flows to zero in the quadrupolar ordered phases, representing a small Fermi surface state [68,69].

To distinguish the critical points and non-Fermi liquid phases experimentally, we compute the zero temperature quadrupolar $\chi_Q(\tau) \sim \tau^{-\gamma_Q}$ and octupolar $\chi_O(\tau) \sim \tau^{-\gamma_O}$ susceptibilities with the exponents γ_Q and γ_O [see Eq. (25) and (26)], where τ is the imaginary time. It is shown that the octupolar susceptibility has different scaling behavior around the non-Fermi liquids and critical fixed points at second order in ϵ, which are summarized in Table I. Finally, we propose how the multipolar susceptibilities can be measured experimentally by the use of ultrasound measurements in the presence of a magnetic field. The temperature/frequency scaling of the

TABLE I. Table of the fixed points and their multipolar susceptibility exponents. $F_{1\pm}$ and $F_{2\pm}$ are the multipolar and 2-channel Kondo fixed points, respectively, and B_Q and B_O are the quadrupolar fixed point and octupolar fixed line, respectively (all four of these are stable). $C_{1,2\pm}^{Q}$ is the critical point between $F_{1,2\pm}$ and B_Q, and $C_{1,2\pm}^{O}$ is the critical point between $F_{1,2\pm}$ and B_O. C_{QO} is the critical point between B_Q and B_O. γ_Q and γ_O stand for the quadrupolar and octupolar suscepti bility exponents defined in Eqs. (25) and (26), respectively. The schematic diagram for their quantum phase transitions is presented in Fig. 1. Note that B_O and $C_{1,2\pm}^{O}$ are outside of the perturbative regime, so their γ_Q values are omitted. Note that in this table, the multipolar susceptibility exponents of $F_{(1,2)\pm}$ are the perturbative values. The exact values from conformal field theory are 2/5 and 1, respectively [47,81].

Label	$(K_{Q1}^*, K_{Q2}^*, K_O^*, \lambda_Q^*, \lambda_O^*)$	Type	γ_Q	γ_O
$F_{1\pm}$	$\left(\pm\frac{1}{2\sqrt{6}}, \pm\frac{1}{12\sqrt{2}}, -\frac{1}{4\sqrt{3}}, 0, 0\right)$	Multipolar	1/2	1/2
$F_{2\pm}$	$\left(\pm\frac{1}{2\sqrt{3}}, \mp\frac{1}{6}, \frac{1}{2\sqrt{3}}, 0, 0\right)$	2-channel Kondo	2	2
B_Q	$\left(0, 0, 0, \epsilon_Q + \epsilon_Q^2, 0\right)$	Quadrupolar	ϵ_Q	$2\epsilon_Q + 2\epsilon_Q^2$
B_O	$\left(0, 0, 0, 0, \infty\right)$	Octupolar	–	ϵ_O
C_{QO}	$\left(0, 0, 0, \frac{\epsilon_Q}{2} + \frac{\epsilon_O(2\epsilon_Q - \epsilon_O)}{4}, \frac{(2\epsilon_Q - \epsilon_O)}{2} + \frac{\epsilon_O^2}{4}\right)$	Critical	ϵ_Q	ϵ_O
$C_{1\pm}^{Q}$	$\left(\pm\frac{\epsilon_Q}{\sqrt{3}}, \pm\frac{\epsilon_Q}{6}, -\frac{\epsilon_Q}{2\sqrt{3}}, \epsilon_Q - 2\epsilon_Q^2, 0\right)$	Critical	ϵ_Q	$2\epsilon_Q$
$C_{2\pm}^{Q}$	$\left(\pm\left(\frac{\epsilon_Q}{2\sqrt{6}} + \frac{\sqrt{3}\epsilon_Q^2}{16\sqrt{2}}\right), \mp\left(\frac{\epsilon_Q}{6\sqrt{2}} + \frac{\epsilon_Q^2}{16\sqrt{2}}\right), \frac{\epsilon_Q}{4\sqrt{3}}, \epsilon_Q + \frac{\epsilon_Q^2}{4}, 0\right)$	Critical	ϵ_Q	$2\epsilon_Q + 3\epsilon_Q^2/2$
$C_{1\pm}^{O}$	$\left(\pm\frac{\epsilon_O^{1/2}}{2\sqrt{3}}, \pm\frac{\epsilon_O^{1/2}}{12}, -\frac{1}{4\sqrt{3}}, 0, \frac{1}{4} - \frac{\epsilon_O}{2}\right)$	Critical	–	ϵ_O
$C_{2\pm}^{O}$	$\left(\pm\frac{\epsilon_O^{1/2}}{2\sqrt{6}}, \mp\frac{\epsilon_O^{1/2}}{6\sqrt{2}}, \frac{1}{2\sqrt{3}}, 0, 1 - \frac{\epsilon_O}{2}\right)$	Critical	–	ϵ_O

multipolar susceptibility is given by $\chi_i'(|\omega/T| \ll 1) \sim T^{\gamma_i - 1}$ and $\chi_i'(|\omega/T| \gg 1) \sim \omega^{\gamma_i - 1}$, respectively, where $i = Q$, O stand for quadrupolar and octupolar, respectively. The elastic constants are directly related to the multipolar susceptibilties, such as $\Delta(C_{11} - C_{12}) \propto \chi_Q'$ and $\Delta C_{44} \propto h^2 \chi_O'$, where ΔC_{ij} is the variation of the elastic constant C_{ij}, and h is the magnetic field. That is, we can obtain the multipolar susceptibility exponent by measuring the temperature dependence of the elastic constants in the presence of the magnetic field using ultrasonic measurements. Our result for the quantum critical behaviors may be realized in experiments on $Pr_2(Ti, V)_2 Al_2$ in the high pressure regime at low temperature.

The remainder of the paper is organized as follows. In Sec. II, we describe modeling the multipolar Kondo lattice in terms of a multipolar Bose-Fermi Kondo model. In Sec. III, we perform a renormalization group analysis of our multipolar Bose-Fermi Kondo model to identify the phases and phase transitions in the model. In Sec. IV, we comment on how these phases can be distinguished experimentally, and in Sec. V we discuss the implications and possible extensions of our work.

II. CONSTRUCTION OF MODELS

We start by describing the microscopic origin of the multipolar moment, and then describe how to construct conduction orbitals. Then, we couple the multipolar impurity to the conduction orbitals which constitutes the (Fermi) Kondo coupling. The Bose-Kondo coupling can then be derived from the Fermi-Kondo coupling by calculating the RKKY coupling of the parent Kondo lattice, and then replacing these other moments with a dynamical bosonic bath field. Since the setting of interest is the prasedoymium cubic compounds $Pr(Ti, V)_2 Al_2 0$, we need to consider the local symmetry of the Pr^{3+} moment. Here, a Pr^{3+} ion rests at the center of a Frank-Kasper cage, which is composed of (Ti, V) and Al. Despite the complicated nature of the cage, its point group symmetry is simply the tetrahedral group T_d. This means that we can classify the wave function of an electron hopping on the cage according to the irreducible representations of T_d. We allow the most general interactions according to the local T_d symmetry and timereversal; the details of the symmetry group are listed in Appendix B.

A. Multipolar moments

Generally speaking, on the site of a local moment, the wave functions of a particular ionic configuration are constrained to an effective ground state by Hund's rules. These ground states are then split by the local crystalline electric field. The consequence of these restrictions is the formation of localized anisotropic charge and magnetization densities, leading to multipolar moments. In the case of a rare-earth Pr^{3+} ion subjected to a tetrahedral (T_d) crystal field, the spin-orbit coupled $J = 4$ multiplet of the $4f^2$ electrons is split to give rise to a low-lying and energetically well-isolated Γ_3 non-Kramers doublet [28]; the doublet states are listed in Appendix A. This Γ_3 doublet supports both time-reversal even quadrupolar moments $\{\mathcal{O}_{22} = \frac{\sqrt{3}}{2}(J_x^2 - J_y^2), \ \mathcal{O}_{20} = \frac{1}{2}(3J_z^2 - \boldsymbol{J}^2)\}$ as well as a timereversal odd octupolar moment $\{\mathcal{T}_{xyz} = \frac{\sqrt{15}}{6}\overline{J_x J_y J_z}\}$; we use the Stevens operators to describe the multipolar moments

and the overline indicates a full symmetrization. These moments can be compactly represented by the pseudospin-1/2 operator $\mathbf{S}$, the components of which are given by [46,54]

$$S^x = -\frac{1}{4}\mathcal{O}_{22}, \quad S^y = -\frac{1}{4}\mathcal{O}_{20}, \quad S^z = \frac{1}{3\sqrt{5}}\mathcal{T}_{xyz}, \quad (1)$$

and satisfy a canonically normalized $\mathfrak{su}(2)$ algebra $[S^i, S^j] = i\epsilon_{ijk}S^k$. Further details of this pseudospin-1/2 object are described in Appendix A. Note that, although the multipolar moments are written in terms of pseudospin-1/2 operators, their transformations under rotations in T_d and time reversal reflect the underlying multipolar attributes.

B. Fermi-Kondo couplings

Wave functions of an electron hopping on a Frank-Kasper cage can be thought of as molecular orbitals centered at the Pr ion. It is these molecular orbitals which we couple to the local multipolar moments described in the previous section. Since these wave functions are classifiable according to irreps of T_d, we pick basis functions for the T_2 representation. Two options are the p-orbital basis functions x, y, z (alternatively, or the T_{2g} orbitals $\{xy, yz, zx\}$ yield an identical model and results). We therefore consider three bands, assumed to be degenerate, constructed from these local orbitals; see Eq. (2). The most general Kondo Hamiltonian couplings of these conduction bands with the local multipolar moments respecting the local T_d symmetry and time-reversal are enumerated in Eqs. (3)–(5) [46,54]:

$$H_0^F = \sum_{\mathbf{k}, \alpha, a} E_{\mathbf{k}} c_{\mathbf{k}a\alpha}^\dagger c_{\mathbf{k}a\alpha}, \quad (2)$$

$$H_{Q1} = K_{Q1} c_{0a\alpha}^\dagger \left(\sigma_{\alpha\beta}^0 \lambda_{ab}^3 S^x - \sigma_{\alpha\beta}^0 \lambda_{ab}^8 S^y\right) c_{0b\beta}, \quad (3)$$

$$H_{Q2} = K_{Q2} c_{0a\alpha}^\dagger \left(2\sigma_{\alpha\beta}^z \lambda_{ab}^2 S^y + \sigma_{\alpha\beta}^y \lambda_{ab}^5 (\sqrt{3}S^x + S^y)\right.$$
$$\left. + \sigma_{\alpha\beta}^x \lambda_{ab}^7 (\sqrt{3}S^x - S^y)\right) c_{0b\beta}, \quad (4)$$

$$H_O = K_O c_{0a\alpha}^\dagger \left(\sigma_{\alpha\beta}^x \lambda_{ab}^6 + \sigma_{\alpha\beta}^y \lambda_{ab}^4 + \sigma_{\alpha\beta}^z \lambda_{ab}^1\right) S^z c_{0b\beta}. \quad (5)$$

The subscript 0 on the conduction electron operators indicates that this interaction occurs only on the impurity site, which is taken to be the origin. The Latin indices sum over orbitals $a, b = x, y, z$, and the Greek indices sum over spins $\alpha, \beta = \uparrow, \downarrow$. σ^i are the standard Pauli matrices, and λ^j are the 3×3 Gell-Mann matrices, listed in Appendix C. For the conduction electrons, we assume a constant density of states near the Fermi surface, $\sum_{\mathbf{k}} \delta(\omega - E_{\mathbf{k}}) = N_0$ between $-D < \omega < D$.

The pseudospin $\mathbf{S}$ represents the multipolar moments, with $S^{x,y}$ and S^z standing for the quadrupolar and octupolar moments, respectively. In order to perform the many-body perturbation theory later in this work, we rewrite the local moment $\mathbf{S}$ in terms of Abrikosov pseudofermions:

$$\mathbf{S} = \sum_{\alpha\beta} f_\alpha^\dagger \frac{\vec{\sigma}_{\alpha\beta}}{2} f_\beta, \quad (6)$$

where we constrain the occupation of the impurity to be $\sum_\alpha f_\alpha^\dagger f_\alpha = 1$. In order to impose this physical constraint, we introduce a chemical potential for the pseudofermion by

adding $\lambda \sum_\sigma f_\sigma^\dagger f_\sigma$ to the Hamiltonian, and take the limit $\lambda \to \infty$ at the end of the calculation [64,77].

C. Bose-Kondo couplings

In the full Kondo lattice, the local Kondo Hamiltonian of Eqs. (3)–(5) appears at each lattice site. Through this Kondo interaction, an effective interaction between local moments is generated, known as the RKKY interaction [78–80]. In the Bose-Fermi Kondo model, this RKKY interaction is represented by the coupling of the local moment to a bosonic bath. The procedure to generate the most general symmetry allowed RKKY-type interaction is described in Appendix D. The resulting kinetic term for bosons and the Bose-Kondo coupling are given in Eqs. (7) and (8), respectively,

$$H_0^B = \sum_{\mathbf{k}} \left[\Omega_{Q\mathbf{k}} \left(\phi_{\mathbf{k}}^{x\dagger} \phi_{\mathbf{k}}^x + \phi_{\mathbf{k}}^{y\dagger} \phi_{\mathbf{k}}^y \right) + \Omega_{O\mathbf{k}} \phi_{\mathbf{k}}^{z\dagger} \phi_{\mathbf{k}}^z \right], \quad (7)$$

$$H_g = g_Q \left(S^x \phi_0^x + S^y \phi_0^y \right) + g_O S^z \phi_0^z. \quad (8)$$

Here, $\Omega_{Q\mathbf{k}}$ and $\Omega_{O\mathbf{k}}$ are the dispersions of the bosonic baths coupled to the quadrupole and octupole moments, respectively. To set up the controlled RG calculation, we introduce an ϵ expansion with dimensional regularization in the density of states of the bosonic bath,

$$\sum_{\mathbf{k}} [\delta(\omega - \Omega_{i,\mathbf{k}}) - \delta(\omega + \Omega_{i,\mathbf{k}})] = \frac{N_i^2}{2} |\omega|^{1-\epsilon_i} \text{sgn}(\omega). \quad (9)$$

To consider the most general situation, we introduce ϵ_Q and ϵ_O for the quadrupolar and octupolar bosonic baths because the density of states power law of the quadrupolar and octupolar bosonic baths are generically different. The multipolar moments localized at $\mathbf{r} = 0$ couple to the bosonic bath fields $\vec{\phi}_0 = \sum_{\mathbf{k}} (\vec{\phi}_{\mathbf{k}} + \vec{\phi}_{-\mathbf{k}}^\dagger)$.

In summary, the total multipolar Bose-Fermi Kondo Hamiltonian H is

$$H = H_0^F + H_{Q1} + H_{Q2} + H_O + H_0^B + H_g. \quad (10)$$

III. RENORMALIZATION GROUP ANALYSIS

A. ϵ-Expansion and Dimensional Regularization

We perform the renormalization group analysis by using dimensional regularization with minimal subtraction [64]. The bosonic bath already has an ϵ factor modifying its density of states which can be used in the minimal subtraction procedure, but the conduction electron bath does not. We therefore introduce ϵ' for the conduction electron density of states to enable the minimal subtraction of poles:

$$\sum_{\mathbf{k}} \delta(\omega - E_{\mathbf{k}}) = N_0 |\omega|^{-\epsilon'}. \quad (11)$$

Note that ϵ' will set to zero at the end of the calculation. Consequently, we define a renormalized field f and dimensionless coupling constants g_i and K_i,

$$f^B = Z_f^{1/2} f, \quad (12)$$

$$g_i^B = g_i Z_f^{-1} Z_{g_i} \mu^{\epsilon_i/2}, \quad (13)$$

$$K_j^B = K_j Z_f^{-1} Z_{K_j} \mu^{\epsilon'}, \quad (14)$$

where μ is the renormalization energy scale, and Z_f, Z_{g_i}, and Z_{K_j} are the renormalization constants for the pseudofermion f, bosonic couplings g_i (here $i = Q, O$), and fermionic couplings K_j (here $j = Q_1, Q_2, O$). The superscript B stands for the bare value which does not evolve under the RG flow. In addition, we absorb the density of states N_i into the dimensionless couplings as $N_0 K_j \to K_j$ and $N_i g_i \to g_i$, respectively, in the following section. The details of the RG analysis and corresponding Feynman diagrams are enumerated in Appendix E. Note that we ignore the self-energies of the conduction electrons and bosonic baths because they vanish in the thermodynamic limit [60].

B. Analysis of the Fermionic Kondo Model

The beta functions with the multipolar moment couplings up to cubic order in K_i are given by [46,47,54]

$$\frac{dK_{Q1}}{d\ln\mu} = 6K_{Q2}K_O + 2K_{Q1}(K_{Q1}^2 + 6K_{Q2}^2 + 3K_O^2), \quad (15)$$

$$\frac{dK_{Q2}}{d\ln\mu} = K_O(K_{Q1} - \sqrt{3}K_{Q2}) + 2K_{Q2}(K_{Q1}^2 + 6K_{Q2}^2 + 3K_O^2), \quad (16)$$

$$\frac{dK_O}{d\ln\mu} = 2K_{Q2}(2K_{Q1} - \sqrt{3}K_{Q2}) + 4K_O(K_{Q1}^2 + 6K_{Q2}^2). \quad (17)$$

This RG flow has two distinct stable fixed points. The two types of stable fixed points are the multipolar fixed points, $F_{1\pm} = (K_{Q1}^*, K_{Q2}^*, K_O^*) = (\pm\frac{1}{2\sqrt{6}}, \pm\frac{1}{12\sqrt{2}}, -\frac{1}{4\sqrt{3}})$, and two-channel Kondo fixed points, $F_{2\pm} = (\pm\frac{1}{2\sqrt{3}}, \mp\frac{1}{6}, \frac{1}{2\sqrt{3}})$. The stable fixed points have perturbative scaling dimensions $\Delta = 1/4$ and $\Delta = 1$, respectively, which are the slope of the beta function at the respective fixed points; both fixed points are non-Fermi liquid phases. Δ is also related to the scaling dimension $(1 + \Delta)$ of the leading irrelevant operator at the fixed point. The physical observables such as resistivity ρ and heat capacity C_V at the fixed points are obtained by using the scaling dimension Δ; at low temperatures we have $\rho \sim T^\Delta$ and $C_V \sim T^{2\Delta}$. Note that the exact scaling dimensions of $F_{1\pm}$ and $F_{2\pm}$ from the CFT are 1/5 and 1/2, respectively [47,54,81].

C. Analysis of the Bosonic Kondo Model

The beta functions for the coupling of the local moment to the bosonic bath up to g_i^5 order are given by

$$\frac{d\lambda_Q}{d\ln\mu} = -\lambda_Q(\epsilon_Q - \lambda_Q - \lambda_O + \lambda_Q^2 + \lambda_Q\lambda_O), \quad (18)$$

$$\frac{d\lambda_O}{d\ln\mu} = -\lambda_O(\epsilon_O - 2\lambda_Q + 2\lambda_Q\lambda_O), \quad (19)$$

where $\lambda_{Q,O} = g_{Q,O}^2$. Equations (18) and (19) have two stable fixed points, a quadrupolar ordered fixed point, $B_Q = (\lambda_Q^*, \lambda_O^*) = (\epsilon_Q + \epsilon_Q^2, 0)$, and an octupolar ordered fixed point, $B_O = (0, \infty)$. The quadrupolar and octupolar fixed points can be identified with an XY fixed point and Ising fixed point in the ordinary Fermi-Bose Kondo model [62,64]. The octupolar fixed point is, strictly speaking, outside of the
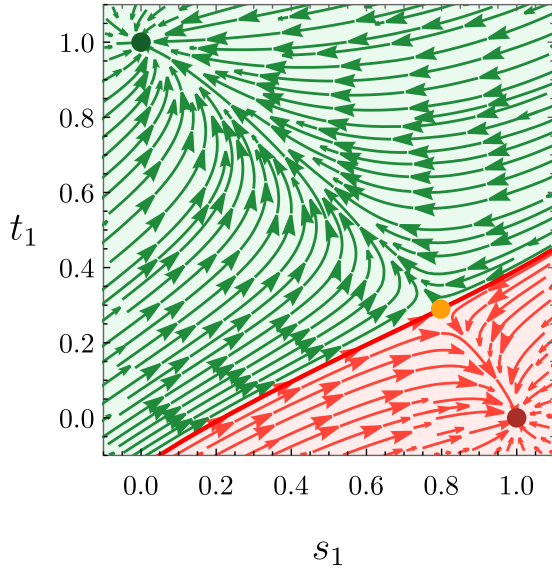
FIG. 2. The RG flow diagram between the multipolar Kondo fixed point F_{1+} (green dot) and quadrupolar fixed point B_Q (red dot) when $\epsilon = 0.1$. F_{1+} and B_Q are located at $(s_1, t_1) = (0, 1)$ and $(s_1, t_1) = (1, 0)$, respectively. Between the two stable fixed points, there is a critical point $C_{1+}^Q = (0.798, 0.289)$ (orange dot), and the red line denotes the separatrix between these two phases. Here, $s_1 = 1 - 0.104 K_{Q1} - 0.180 K_{Q2} + 6.708 K_O$, $t_1 = 3.796 K_{Q1} + 6.574 K_{Q2} + 1.124 K_O$, and $\lambda_O = 0$, with the constraint $\lambda_Q = 0.113 - 0.571 K_{Q1} - 0.989 K_{Q2} - 0.430 K_O$.
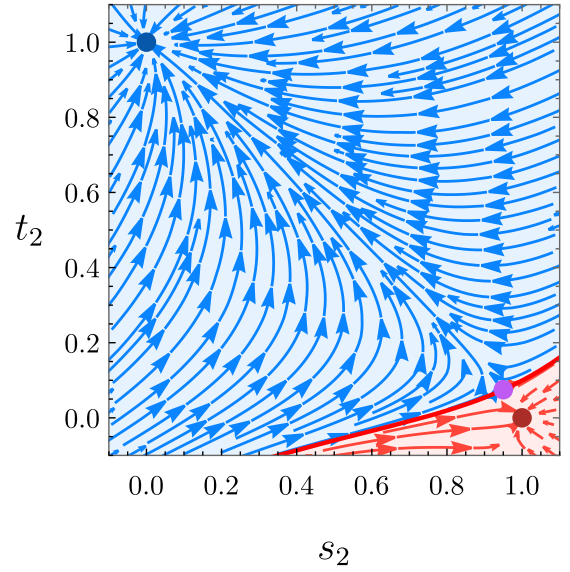
FIG. 3. The RG flow diagram between the 2-channel Kondo fixed point F_{2+} [blue dot, $(s_2, t_2) = (0, 1)$] and quadrupolar fixed point B_Q [red dot, $(s_2, t_2) = (1, 0)$] when $\epsilon = 0.1$. Between the two fixed points, there is a critical point $C_{2+}^Q = (0.950, 0.075)$ (purple dot). The red line denotes the separatrix between the two phases. Here, $s_2 = 1 - 0.003 K_{Q1} + 0.011 K_{Q2} - 3.455 K_O$, $t_2 = 1.219 K_{Q1} - 4.222 K_{Q2} - 0.192 K_O$, and $\lambda_O = 0$ with the constraint $\lambda_Q = 0.113 - 0.218 K_{Q1} + 0.755 K_{Q2} + 0.263 K_O$.

regime of our perturbative calculation. The beta functions also have another fixed point, $C_{QO} = (\frac{\epsilon_Q}{2} + \frac{\epsilon_O(2\epsilon_Q - \epsilon_O)}{4}, \frac{(2\epsilon_Q - \epsilon_O)}{2} + \frac{\epsilon_O^2}{4})$, which is a critical point between the quadrupolar and octupolar fixed points, and corresponds to the XXZ fixed point in the ordinary Fermi-Bose Kondo model [62,64]. All the fixed point values are calculated up to ϵ_i^2 order. In the limit $\epsilon_Q = \epsilon_O = \epsilon$, $C_{QO} = (\frac{\epsilon}{2} + \frac{\epsilon^2}{4}, \frac{\epsilon}{2} + \frac{\epsilon^2}{4})$ becomes isotropic [62,64]. Note that B_Q exists in the range $0 < \epsilon_Q < 1/4$, and C_{QO} exists when $27\epsilon_O^2 - 2(2 + \epsilon_O - 2\epsilon_Q)^3 < 0$ and $\epsilon_Q \gtrsim \sqrt{3.516 + 2\epsilon_O - \epsilon_O^2} - 1.875$ with $0 < \epsilon_O < 1$. For the isotropic limit $\epsilon = \epsilon_Q = \epsilon_O$, the range is $0 < \epsilon < 1/2$.

D. Analysis of the Bose-Fermi Kondo Model

In order to study the destruction of the Kondo effect to magnetic ordering, we consider the full model of coupling the local moment to both the fermionic conduction electron bath and the bosonic bath. In this case, the beta functions are as follows:

$$
\frac{dK_{Q1}}{d \ln \mu} = K_{Q1}\left(\frac{\lambda_Q + \lambda_O}{2} - \frac{\lambda_Q(\lambda_Q + \lambda_O)}{2}\right) + 6K_{Q2}K_O + 2K_{Q1}(K_{Q1}^2 + 6K_{Q2}^2 + 3K_O^2),
$$
(20)

$$
\frac{dK_{Q2}}{d \ln \mu} = K_{Q2}\left(\frac{\lambda_Q + \lambda_O}{2} - \frac{\lambda_Q(\lambda_Q + \lambda_O)}{2}\right) + K_O(K_{Q1} - \sqrt{3}K_{Q2}) + 2K_{Q2}(K_{Q1}^2 + 6K_{Q2}^2 + 3K_O^2),
$$
(21)

$$
\frac{dK_O}{d \ln \mu} = K_O(\lambda_Q - \lambda_Q\lambda_O) + 2K_{Q2}(2K_{Q1} - \sqrt{3}K_{Q2}) + 4K_O(K_{Q1}^2 + 6K_{Q2}^2),
$$
(22)

$$
\frac{d\lambda_Q}{d \ln \mu} = -\lambda_Q[\epsilon_Q - (\lambda_Q + \lambda_O) + \lambda_Q(\lambda_Q + \lambda_O) - 4(K_{Q1}^2 + 6K_{Q2}^2 + 3K_O^2)],
$$
(23)

$$
\frac{d\lambda_O}{d \ln \mu} = -\lambda_O[\epsilon_O - 2\lambda_Q + 2\lambda_Q\lambda_O - 8(K_{Q1}^2 + 6K_{Q2}^2)].
$$
(24)

Under this full renormalization group flow, all of the previously found stable fixed points in the fermionic Kondo $F_{1\pm}$, $F_{2\pm}$ and bosonic Kondo B_Q, and B_O cases remain stable. Further, new fixed points emerge, which describe critical points between the phases described in Secs. III B and III C. For the case $\lambda_Q \neq 0$, $\lambda_O = 0$, we find two pairs of critical points. The first critical point is given by $C_{1\pm}^Q = (K_{Q1}^*, K_{Q2}^*, K_O^*, \lambda_Q^*, \lambda_O^*) = (\pm\frac{\epsilon_Q}{\sqrt{3}}, \pm\frac{\epsilon_Q}{6}, -\frac{\epsilon_Q}{2\sqrt{3}}, \epsilon_Q - 2\epsilon_Q^2, 0)$ which is a critical point between $F_{1\pm}$ and B_Q. The flow diagram corresponding to this transition is given in Fig. 2. The second critical point is $C_{2\pm}^Q = (\pm(\frac{\epsilon_Q}{2\sqrt{6}} + \frac{\sqrt{3}\epsilon_Q^2}{16\sqrt{2}}), \mp(\frac{\epsilon_Q}{6\sqrt{2}} + \frac{\epsilon_Q^2}{16\sqrt{2}}), \frac{\epsilon_Q}{4\sqrt{3}}, \epsilon_Q + \frac{\epsilon_Q^2}{4}, 0)$. This is a critical point between $F_{2\pm}$ and B_Q, and its flow diagram is Fig. 3. In the case of $\lambda_Q = 0$, $\lambda_O \neq 0$, we find the critical points, $C_{1,2\pm}^O$, between $F_{1,2\pm}$ and B_O. However, the fixed point values of λ_O in B_O and $C_{1,2\pm}^O$ are order one numbers, so they are outside of the perturbative regime. Despite this, we

believe the existence of the fixed points to be maintained under specialized nonperturbative methods. For example, the octupolar-type critical points may be accessible via the Coulomb gas representation [56,64]. Note that $C_{1\pm}^{Q,O}$ and $C_{2\pm}^{Q,O}$ exist for $0 < \epsilon_Q < 1/2$ and $0 < \epsilon_Q < 2 - \sqrt{2}$, respectively.

IV. PHYSICAL OBSERVABLES

A. Multipolar Susceptibility and Exponents

In order to compare our results with the experiment, we consider the local multipolar moment susceptibility exponent. The local quadrupolar and octupolar moment susceptibilities, χ_Q and χ_O, are defined as

$$\chi_Q(\tau) = \langle T_\tau S^{x,y}(\tau) S^{x,y}(0) \rangle \propto \left(\frac{\tau_0}{|\tau|} \right)^{\gamma_Q}, \quad (25)$$

$$\chi_O(\tau) = \langle T_\tau S^z(\tau) S^z(0) \rangle \propto \left(\frac{\tau_0}{|\tau|} \right)^{\gamma_O}, \quad (26)$$

where γ_i $(i = Q, O)$ is the multipolar susceptibility exponent and $\tau \gg \tau_0$ with the cutoff $\tau_0 = 1/\Lambda$. We emphasize that the multipolar susceptibility exponents describe how the susceptibility scales as imaginary time evolves, but do not directly yield the temperature scaling. When the fixed point value of λ_i $(i = Q, O)$ is nonzero, the corresponding susceptibility exponent is given by [62,64]

$$\gamma_i = \epsilon_i + \left[\frac{1}{\lambda_i} \frac{d\lambda_i}{d \ln \mu} \right]_{\text{f.p.}}, \quad (27)$$

where f.p. stands for value at the fixed point. By definition, $\frac{d\lambda_i}{d \ln \mu} = 0$ is at the fixed point, so $\gamma_i = \epsilon_i$, which is exact to all orders of ϵ [62,64]. Since our critical points $C_{1,2\pm}^Q$ all have a nonzero fixed point value for λ_Q, the quadrupolar susceptibility exponent of the critical points $C_{1\pm}^Q$ and $C_{2\pm}^Q$ are both given by $\gamma_Q = \epsilon_Q$. Thus we cannot distinguish between the two critical points via γ_Q. Let us consider instead the case of the octupolar susceptibility exponent.

When the fixed point value of λ_i is zero, as is the case for λ_O at both $C_{1,2\pm}^Q$, then the corresponding susceptibility exponent is given by [62]

$$\gamma_i = \epsilon_i + \left[\lim_{\lambda_i \to 0} \frac{1}{\lambda_i} \frac{d\lambda_i}{d \ln \mu} \right]_{\text{f.p.}}$$

$$= \epsilon_i + \left[\frac{\partial}{\partial \lambda_i} \frac{d\lambda_i}{d \ln \mu} \right]_{\text{f.p.}}. \quad (28)$$

In contrast to the previous case, Eq. (28) includes higher order corrections in $\epsilon_{Q,O}$. Since our calculation applies to order ϵ^2, we can use ϵ^2 corrections to the octupolar susceptibility to distinguish between different fixed points. The resulting susceptibilities for the two critical points are $\gamma_O = 2\epsilon_Q$ and $2\epsilon_Q + 3\epsilon_Q^2/2$, for $C_{1\pm}^Q$ and $C_{2\pm}^Q$, respectively. The results for the susceptibility exponents at different fixed points are summarized at Table I. The full expression of the multipolar susceptibility exponent γ_i for $\lambda_i^* = 0$ is presented in Appendix F. An additional point is that we may also distinguish between these critical points and the non-Fermi liquid phases $F_{1\pm}$ and $F_{2\pm}$ using this octupolar susceptibility. This is useful because we can then distinguish non-Fermi liquid behavior due to a

quantum critical regime from non-Fermi liquid behavior in a phase ($F_{1\pm}$ or $F_{2\pm}$ in our case). We note that the multipolar susceptibility exponents of the fermionic fixed points $F_{(1,2)\pm}$ are perturbative. The exact exponents can be obtained via conformal field theory and are 2/5 and 1 for $F_{1\pm}$ and $F_{2\pm}$, respectively [47,81].

B. Finite Temperature Scaling and Elastic Constants

The results in the previous section only apply at zero temperature, and do not directly correspond to a measurable quantity. In order to obtain the temperature dependence of the susceptibility, we assume that we have conformal invariance at the critical point, and that the multipolar moment is a primary operator with conformal dimension $\gamma_i/2$ [62,82]. The results for the real part χ' and imaginary part χ'' are given by Eqs. (29) and (30); see Appendix G for details.

$$\chi_i'(\omega, T) \propto \begin{cases} T^{\gamma_i - 1}\left(1 + C_{\text{Re}1}\left(\frac{\omega}{T}\right)^2\right), & |\omega| \ll T, \\ \omega^{\gamma_i - 1}, & |\omega| \gg T, \end{cases} \quad (29)$$

$$\chi_i''(\omega, T) \propto \begin{cases} T^{\gamma_i - 1}\left(\frac{\omega}{T}\right), & |\omega| \ll T, \\ \omega^{\gamma_i - 1}, & |\omega| \gg T, \end{cases} \quad (30)$$

where $C_{\text{Re}1}$ is defined in Appendix G. Note that the real part of the temperature dependence of the multipolar susceptibility for $F_{1\pm}$ and $F_{2\pm}$ in the dc limit ($\omega = 0$) is consistent with the temperature scaling, $\chi \sim T^{2\Delta - 1}$, which is the conformal field theory result upon setting $\gamma_i = 2\Delta$ [81]. The exact temperature dependencies for $F_{1\pm}$ and $F_{2\pm}$ from CFT are given by $\chi \sim T^{-3/5}$ and $\chi \sim \log T$, respectively [47]. We expect that the multipolar susceptibility exponent in Eq. (29) can be observed by measuring the temperature dependence of elastic constants [83,84]. The elastic free energy including the symmetry-allowed coupling between the multipolar moments and strains is given by [49,84]

$$\mathcal{F} = \frac{C_{11}^0 - C_{12}^0}{2}(\epsilon_\mu^2 + \epsilon_\nu^2) + \frac{C_{44}^0}{2}(\epsilon_{xy}^2 + \epsilon_{yz}^2 + \epsilon_{zx}^2)$$
$$- s_Q[\epsilon_\mu \mathcal{O}_{22} + \epsilon_\nu \mathcal{O}_{20}]$$
$$- s_O \mathcal{T}_{xyz}[h_x \epsilon_{yz} + h_y \epsilon_{zx} + h_z \epsilon_{xy}], \quad (31)$$

where ϵ_{ij} is the strain tensor, $\epsilon_\mu \equiv (\epsilon_{xx} - \epsilon_{yy})$ and $\epsilon_\nu \equiv (2\epsilon_{zz} - \epsilon_{xx} - \epsilon_{yy})/\sqrt{3}$, C_{11}, C_{12}, and C_{44} are the elastic constants which are coefficients of ϵ_{ii}^2, $\epsilon_{ii}\epsilon_{jj}$, and ϵ_{ij}^2 $(i \neq j)$ for the deformation free energy in the cubic lattice, respectively; h_i is the magnetic field $(i = x, y, z)$; the superscript 0 stands for the bare value of the elastic constants; s_Q and s_O are the couplings between the multipolar moments and lattice strain tensors. From second-order perturbation theory, we can get the following corrections to the bare elastic constants,

$$(C_{11} - C_{12}) = (C_{11}^0 - C_{12}^0) - (s_Q^2)\chi_Q', \quad (32)$$

$$C_{44} = C_{44}^0 - (s_O^2 h_i^2)\chi_O', \quad (33)$$

where we apply the magnetic field h_i along one and only one of the x, y, or z axes under the assumption that the cubic symmetry is negligibly affected. The octupolar susceptibility is therefore only detectable when measured in the presence of both strain and magnetic field simultaneously. As a result, the multipolar susceptibility can be observed by measuring

the temperature dependence of the elastic constants $(C_{11}-C_{12})$ and C_{44} via ultrasonic measurements.

V. CONCLUSIONS

Inspired by experiments on Pr(Ti, V)$_2$Al$_2$0, we have studied an appropriate multipolar Bose-Fermi Kondo model, where the non-Kramers local moments carrying quadrupolar and octupolar moments are coupled to p-orbital electrons. By using an RG analysis on our model, we find not only two non-Fermi liquid phases and a quadrupolar ordered phase, but also two quantum critical points between the non-Fermi liquid phases and quadrupolar ordered phase. To distinguish between each of these non-Fermi liquid phases and quantum critical points, we compute the multipolar susceptibility exponents at zero temperature and show that the octupolar susceptibility exponent is different at second order in ϵ at all of these fixed points. Furthermore, we obtain the temperature scaling behavior of the multipolar susceptibility, and explain how the quadrupolar and octupolar susceptibilities are related to the elastic constants $(C_{11}\text{-}C_{12})$ and C_{44}, respectively. We propose that measurement of the temperature dependence of the elastic constants $(C_{11}\text{-}C_{12})$ and C_{44} using an ultrasonic measurement in the presence of a magnetic field can be used to distinguish the non-Fermi liquid phases and quantum critical points experimentally. Our results may be experimentally relevant for Pr$_2$(Ti, V)$_2$Al$_2$ in the high-pressure regime at low temperature.

Possible directions for future work could include applying the work to a variety of other heavy fermion systems. For example, several Yb and Ce compounds exhibit local moments with very high degeneracies, which enables the formation of a large number of multipolar moments [3,4,15,85–90]. Another direction could be to verify our results from the (extended) dynamical mean field theory perspective. One subtlety is that the ϵ_Q, ϵ_O parameters in the bosonic bath density of states should be determined self-consistently, which may be possible in a full dynamical mean field treatment [58].

More generally, our results are indicative of the large variety of multipolar ordered phases and exotic electronic states found in rare-earth metallic systems. The root of the multipolar moments, unusual Kondo couplings, and anisotropic RKKY interactions is the strong spin-orbit coupling and crystal electric field effects, which, as we have shown, can lead to a myriad of quantum critical behaviors. This suggests there may be new classes of quantum critical points relating Kondo destruction, multipolar ordering, and non-Fermi liquids in multipolar Kondo lattice systems, and that they are experimentally accessible. This opens new doors for exploring the landscape of multipolar quantum matter.

APPENDIX A: MULTIPOLAR MOMENTS FROM NON-KRAMERS DOUBLET

In a vacuum, a Pr^{3+} ion forms a spin $J = 4$ system by Hund's rules. In the presence of a tetrahedral crystal field, these nine degenerate states are split, and the resulting ground state in the Pr(V, Ti)$_2$Al$_{20}$ compounds is a non-Kramers Γ_3 doublet spanned by the following two states [28,46,54]:

$$|\Gamma_3^{(1)}\rangle = \frac{1}{2}\sqrt{\frac{7}{6}}|4\rangle - \frac{1}{2}\sqrt{\frac{5}{3}}|0\rangle + \frac{1}{2}\sqrt{\frac{7}{6}}|-4\rangle, \quad \text{(A1)}$$

$$|\Gamma_3^{(2)}\rangle = \frac{1}{\sqrt{2}}|2\rangle + \frac{1}{\sqrt{2}}|-2\rangle. \quad \text{(A2)}$$

To determine which multipolar moments are supported by these wave functions, we can compute the matrix elements of Stevens operators in the doublet $\{|\Gamma_3^{(1)}\rangle, |\Gamma_3^{(2)}\rangle\}$. In this doublet, we find that, defining a different basis

$$|\uparrow\rangle = \frac{1}{\sqrt{2}}\big(|\Gamma_3^{(1)}\rangle + i|\Gamma_3^{(2)}\rangle\big), \quad \text{(A3)}$$

$$|\downarrow\rangle = \frac{1}{\sqrt{2}}\big(i|\Gamma_3^{(1)}\rangle + |\Gamma_3^{(2)}\rangle\big), \quad \text{(A4)}$$

we find that

$$\langle\alpha|\left(-\frac{1}{4}\mathcal{O}_{22}\right)|\beta\rangle = \frac{1}{2}\sigma_{\alpha\beta}^x, \quad \text{(A5)}$$

$$\langle\alpha|\left(-\frac{1}{4}\mathcal{O}_{20}\right)|\beta\rangle = \frac{1}{2}\sigma_{\alpha\beta}^y, \quad \text{(A6)}$$

$$\langle\alpha|\left(\frac{1}{3\sqrt{5}}\mathcal{T}_{xyz}\right)|\beta\rangle = \frac{1}{2}\sigma_{\alpha\beta}^z, \quad \text{(A7)}$$

where α, β take the values $\uparrow, \downarrow$ [where these $\uparrow, \downarrow$ are the ones listed in Eqs. (A3) and (A4)], and σ^i are the standard Pauli matrices. We emphasize that these σ^i matrices and indices α, β relate to matrix elements of operators in local moment states, and have nothing to do with the Pauli matrices and α, β indices for the conduction electrons in Eqs. (3)–(5).

APPENDIX B: ACTION OF TETRAHEDRAL GROUP

In order to test which terms in the Hamiltonian are allowed, we need to know how candidate terms transform under action of the tetrahedral group T_d, and under time-reversal $\mathcal{T}$. The most economical way to check all transformations is to pick two generators of T_d, which are $\mathcal{C}_{31}$ and $\mathcal{S}_{4z}$. $\mathcal{C}_{31}$ is the rotation by $2\pi/3$ about the $(1,1,1)$ axis, and $\mathcal{S}_{4z}$ is a rotation by $\pi/2$ about the $z$axis followed by a mirror reflection across the xy plane. Both of these transformations leave a tetrahedron invariant. Checking all possible Kondo terms respecting the symmetry yields in Eqs. (3)–(5). The table of all symmetry transformation is given by Table II.

APPENDIX C: SU(3) GELL-MANN MATRICES

In our multipolar Kondo models, we have three orbitals. To account for all possible traceless hermitian matrices which describe possible fermionic bilinears, we use the generators of SU(3), normalized to tr$(\lambda^i\lambda^j) = 2\delta_{ij}$. We enumerate these 3×3 Gell-Mann matrices that appear in the Fermi-Kondo

TABLE II. Symmetry transformations of various objects under two generators of the tetrahedral group as well as time-reversal $\mathcal{T}$.

Object	$\mathcal{S}_{4z}$	$\mathcal{C}_{31}$	$\mathcal{T}$
x	$-y$	y	x
y	x	z	y
z	$-z$	x	z
σ^0	σ^0	σ^0	σ^0
σ^x	σ^y	σ^y	$-\sigma^x$
σ^y	$-\sigma^x$	σ^z	$-\sigma^y$
σ^z	σ^z	σ^x	$-\sigma^z$
S^x	$-S^x$	$-\frac{1}{2}S^x - \frac{\sqrt{3}}{2}S^y$	S^x
S^y	S^y	$\frac{\sqrt{3}}{2}S^x - \frac{1}{2}S^y$	S^y
S^z	$-S^z$	S^z	$-S^z$

Hamiltonians here [46,54]:

$$\lambda^1 = \begin{pmatrix} 0 & 1 & 0 \\ 1 & 0 & 0 \\ 0 & 0 & 0 \end{pmatrix}, \quad \lambda^2 = \begin{pmatrix} 0 & -i & 0 \\ i & 0 & 0 \\ 0 & 0 & 0 \end{pmatrix}, \tag{C1}$$

$$\lambda^3 = \begin{pmatrix} 1 & 0 & 0 \\ 0 & -1 & 0 \\ 0 & 0 & 0 \end{pmatrix}, \quad \lambda^4 = \begin{pmatrix} 0 & 0 & 1 \\ 0 & 0 & 0 \\ 1 & 0 & 0 \end{pmatrix}, \tag{C2}$$

$$\lambda^5 = \begin{pmatrix} 0 & 0 & -i \\ 0 & 0 & 0 \\ i & 0 & 0 \end{pmatrix}, \quad \lambda^6 = \begin{pmatrix} 0 & 0 & 0 \\ 0 & 0 & 1 \\ 0 & 1 & 0 \end{pmatrix}, \tag{C3}$$

$$\lambda^7 = \begin{pmatrix} 0 & 0 & 0 \\ 0 & 0 & -i \\ 0 & i & 0 \end{pmatrix}, \quad \lambda^8 = \frac{1}{\sqrt{3}}\begin{pmatrix} 1 & 0 & 0 \\ 0 & 1 & 0 \\ 0 & 0 & -2 \end{pmatrix}. \tag{C4}$$

APPENDIX D: BOSE-KONDO COUPLING

In order to construct the coupling of the local moment to the bosonic bath while respecting the local symmetry, we construct the effective interaction between spins in the corresponding Kondo lattice. Starting with the Fermi-Kondo Hamiltonian in Eqs. (3)–(5), we can compute the effective interaction between two spins by computing the diagram in Fig. 4. We then replace one of the spin operators in this resulting RKKY interaction with the bosonic field and thereby find the symmetry-allowed coupling of the local moment to the bosonic bath. We emphasize that this is not an actual
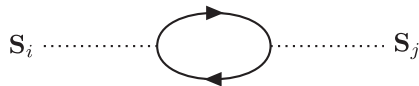
FIG. 4. Effective Kondo Lattice RKKY Interaction; dotted lines refer to the pseudospin operators (not to be confused with dashed lines in other diagrams referring to pseudofermion propagators) and the solid lines are fermion propagators. The $\mathbf{S}_i$ and $\mathbf{S}_j$ are the spin operators on different sites i and j in the parent Kondo lattice.
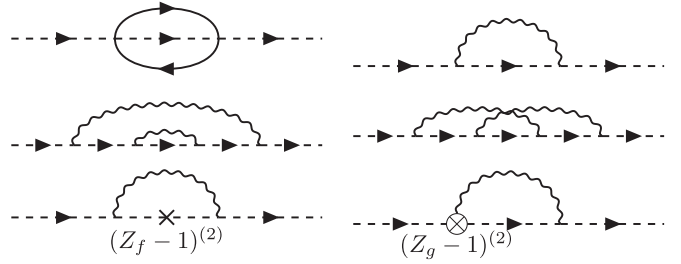
FIG. 5. Pseudofermion self-energy, both direct and counterterm contribution.

RKKY interaction between local moments on different sites, and should be conceptually likened to a Weiss mean field coupled to the impurity.

APPENDIX E: DETAILS OF THE RENORMALIZATION GROUP METHOD

From the bare Hamiltonian presented in the main text, we can introduce counterterms in order to remove divergences in the loop integrals. When calculating the Fermi-Kondo and Bose-Kondo vertex functions, as well as the pseudofermion self-energy, we can solve for these counterterms order by order and use them to compute the renormalization factors. The corresponding diagrams for the pseudofermion self-energy are given in Fig. 5, the diagrams for the Fermi-Kondo vertex corrections are given in Figs. 6–11, and the diagrams for the Bose-Kondo vertex corrections are given in Figs. 12 and 13. Details for how to extract renormalization constants from the vertex corrections and self-energy are presented in an excellent reference [64]. In the Feynman diagrams of Figs. 5–13, solid lines refer to conduction electron propagators [Eq. (E1)], dashed lines corresponds to pseudofermion propagators [Eq. (E2)], and the squiggly lines refer to bosonic bath propagators [Eq. (E3)]:

$$\mathcal{G}_0^c(i\omega, \mathbf{k}) = \frac{1}{i\omega - E_{\mathbf{k}}}, \tag{E1}$$

$$\mathcal{G}_0^f(i\omega, \mathbf{k}) = \frac{1}{i\omega - \lambda}, \tag{E2}$$

$$\mathcal{G}_0^\phi(i\omega, \mathbf{k}) = \frac{2\Omega_{\mathbf{k}}}{(i\omega - \Omega_{\mathbf{k}})(i\omega + \Omega_{\mathbf{k}})}. \tag{E3}$$
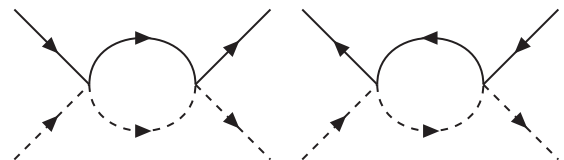
FIG. 6. Order K corrections to the Fermi-Kondo vertex. There are only direct contributions at this order.
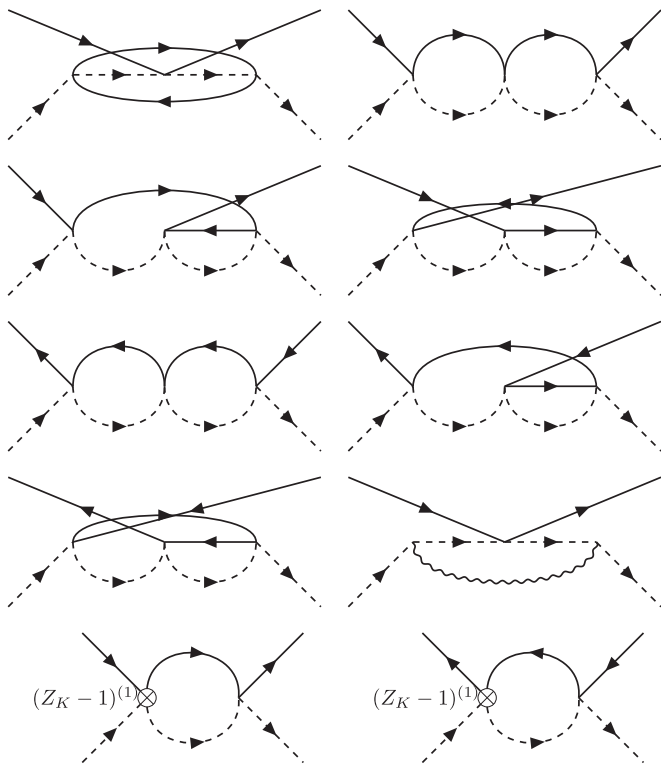
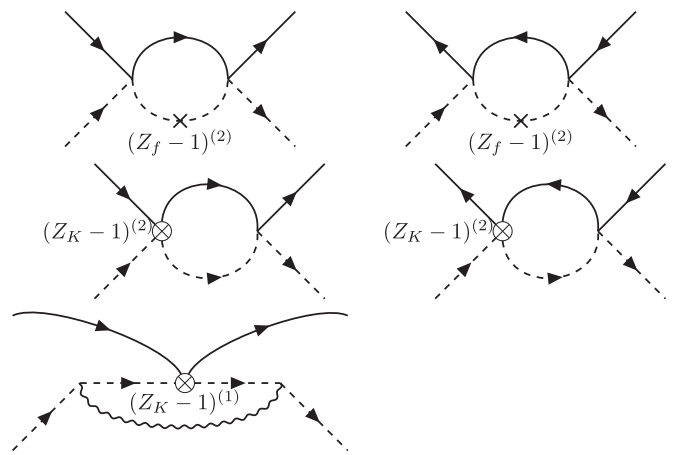FIG. 7. Order K^2 and g^2 corrections to the Fermi-Kondo vertex.

FIG. 9. Order Kg^2 counterterm corrections to the Fermi-Kondo vertex.
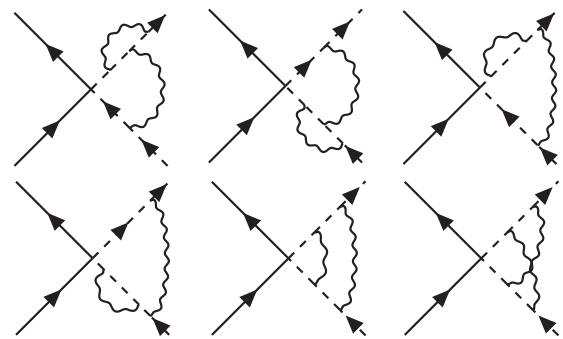

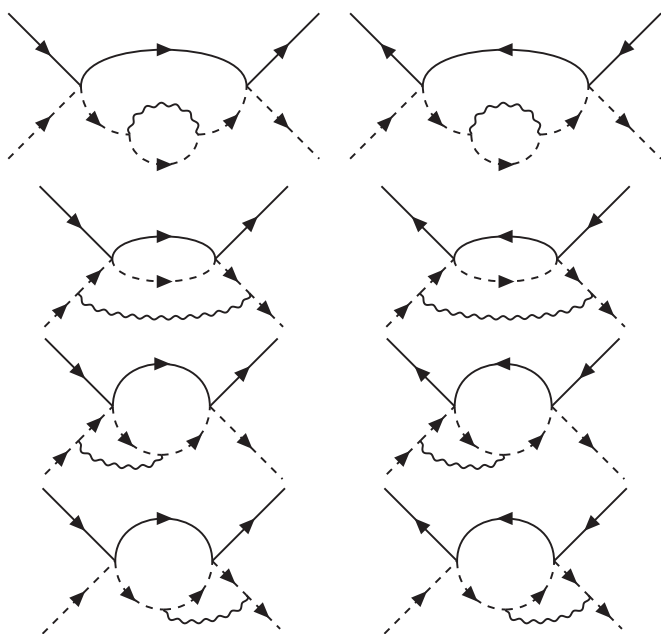FIG. 10. Order g^4 direct corrections to the Fermi-Kondo vertex.

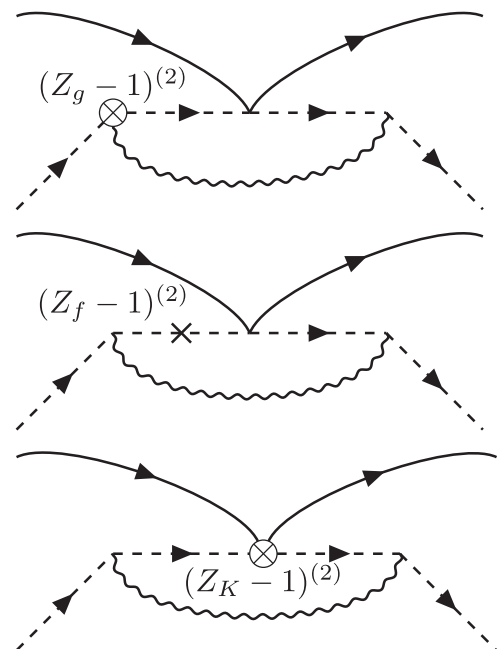FIG. 8. Order Kg^2 direct correction to the Fermi-Kondo vertex.
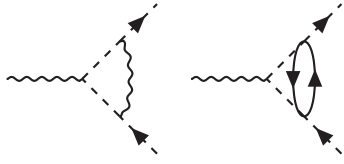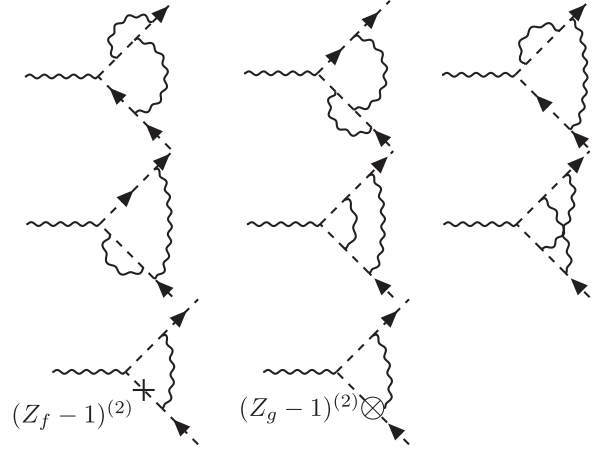

FIG. 11. Order g^4 counterterm corrections to the Fermi-Kondo vertex.

FIG. 12. Order g^2 and K^2 corrections to the Bose-Kondo vertex.

FIG. 13. Order g^4 direct and counterterm corrections to the Bose-Kondo vertex.

The renormalization constants and wavefunction renormalization up to third order in K_i and fifth order in g_i, are given in Eqs. (E4)–(E9).

$$Z_{K_{Q1}} = 1 - \frac{1}{\epsilon_Q} \frac{g_Q^2(g_Q^2 - g_O^2)}{8} + \frac{1}{\epsilon_O}\left[\frac{g_O^2}{4} + \frac{g_O^2 g_Q^2}{8}\right] + \frac{1}{\epsilon_O^2}\frac{g_O^4}{32} + \frac{1}{\epsilon_Q \epsilon_O}\frac{3g_Q^2 g_O^2}{8} + \frac{1}{\epsilon_O \epsilon'}\frac{3K_{Q2}K_O g_O^2}{2K_{Q1}} + \frac{1}{\epsilon'}\left[\frac{3K_O^2}{2} + \frac{6K_{Q2}K_O}{K_{Q1}}\right]$$
$$+ \frac{1}{\epsilon'^2}\left[12K_{Q2}^2 + 3K_O^2 - \frac{3\sqrt{3}K_{Q2}}{K_{Q1}}\left(2K_{Q2}^2 + K_O^2\right) + \frac{9K_{Q2}K_O}{K_{Q1}}\left(4K_{Q2}^2 + K_O^2\right)\right]$$
$$- \frac{1}{\epsilon_Q(\epsilon_Q + \epsilon_O)}\frac{g_Q^2 g_O^2}{4} + \frac{1}{\epsilon'(\epsilon_Q + \epsilon')}\frac{6K_{Q2}K_O g_Q^2}{K_{Q1}}, \tag{E4}$$

$$Z_{K_{Q2}} = 1 - \frac{1}{\epsilon_Q} \frac{g_Q^2(g_Q^2 - g_O^2)}{8} + \frac{1}{\epsilon_O}\left[\frac{g_O^2}{4} + \frac{g_O^2 g_Q^2}{8}\right] + \frac{1}{\epsilon_O^2}\frac{g_O^4}{32} + \frac{1}{\epsilon_Q \epsilon_O}\frac{3g_Q^2 g_O^2}{8} + \frac{1}{\epsilon_O \epsilon'}\left[\frac{K_{Q1}K_O g_O^2}{4K_{Q2}} - \frac{\sqrt{3}K_O g_O^2}{4}\right]$$
$$+ \frac{1}{\epsilon'}\left[\frac{K_{Q1}K_O}{K_{Q2}} - \sqrt{3}K_O + \frac{3K_O^2}{2}\right] + \frac{1}{\epsilon'^2}\left[2K_{Q1}^2 + 3K_{Q2}^2 + \frac{9K_O^2}{2} - 3\sqrt{3}K_{Q1}K_{Q2} - \frac{\sqrt{3}K_{Q1}K_O^2}{K_{Q2}}\right.$$
$$\left. + K_O\left(-\sqrt{3}K_{Q1}^2 + 6K_{Q1}K_{Q2} - 6\sqrt{3}K_{Q2}^2 - \frac{3\sqrt{3}K_O^2}{2}\right) + \frac{K_{Q1}K_O}{2K_{Q2}}\left(2K_{Q1}^2 + 3K_O^2\right)\right]$$
$$- \frac{1}{\epsilon_Q(\epsilon_Q + \epsilon_O)}\frac{g_Q^2 g_O^2}{4} + \frac{1}{\epsilon'(\epsilon_Q + \epsilon')}\left[\frac{K_{Q1}K_O g_Q^2}{K_{Q2}} - \sqrt{3}K_O g_Q^2\right], \tag{E5}$$

$$Z_{K_O} = 1 + \frac{1}{\epsilon_Q}\left[\frac{g_Q^2}{2} + \frac{g_Q^4}{8} + \frac{g_Q^2 g_O^2}{4}\right] + \frac{1}{\epsilon_Q^2}\frac{3g_Q^4}{8} - \frac{1}{\epsilon_O}\frac{g_O^2 + g_Q^2 g_O^2}{4} + \frac{1}{\epsilon_O^2}\frac{g_O^4}{32} - \frac{1}{\epsilon_Q \epsilon_O}\frac{3g_Q^2 g_O^2}{8} + \frac{1}{\epsilon_O \epsilon'}\left[-\frac{K_{Q1}K_{Q2}g_O^2}{K_O} + \frac{\sqrt{3}K_{Q2}^2 g_O^2}{K_O}\right]$$
$$+ \frac{1}{\epsilon_Q \epsilon'}\left[\frac{2K_{Q1}K_{Q2}g_Q^2}{K_O} - \frac{\sqrt{3}K_{Q2}^2 g_Q^2}{K_O}\right] + \frac{1}{\epsilon'}\left[K_{Q1}^2 + 6K_{Q2}^2 - \frac{3K_O^2}{2} + \frac{2K_{Q2}}{K_O}(2K_{Q2} - \sqrt{3}K_{Q2})\right]$$
$$+ \frac{1}{\epsilon'^2}\left[2K_{Q1}^2 - 4\sqrt{3}K_{Q1}K_{Q2} + 18K_{Q2}^2 + 3K_{Q2}K_O(2K_{Q1} - \sqrt{2}K_{Q2}) + \frac{2K_{Q2}}{K_O}(K_{Q1}^2 + 6K_{Q2}^2)(2K_{Q1} - \sqrt{3}K_{Q2})\right]$$
$$- \frac{1}{\epsilon_Q(\epsilon_Q + \epsilon_O)}\frac{g_Q^2 g_O^2}{4} + \frac{1}{\epsilon'(\epsilon_Q + \epsilon')}\left[\frac{K_{Q1}K_O g_Q^2}{K_{Q2}} - \sqrt{3}K_O g_Q^2\right], \tag{E6}$$

$$Z_{g_Q} = 1 - \frac{1}{\epsilon_Q}\frac{g_Q^2(g_Q^2 + g_O^2)}{8} + \frac{1}{\epsilon_O}\left[\frac{g_O^2}{4} + \frac{g_Q^2 g_O^2}{8}\right] + \frac{1}{\epsilon_O^2}\frac{g_O^4}{32} + \frac{1}{\epsilon'}\frac{3K_O^2}{2} + \frac{1}{\epsilon_Q \epsilon_O}\frac{3g_Q^2 g_O^2}{8} - \frac{1}{\epsilon_Q(\epsilon_Q + \epsilon_O)}\frac{g_Q^2 g_O^2}{4}, \tag{E7}$$

$$Z_{go} = 1 + \frac{1}{\epsilon_Q}\left[\frac{g_Q^2}{2} + \frac{g_Q^4}{8} + \frac{g_Q^2 g_O^2}{4}\right] + \frac{1}{\epsilon_Q^2}\frac{3g_Q^4}{8} - \frac{1}{\epsilon_O}\frac{(g_O^2 + g_Q^2 g_O^2)}{4} + \frac{1}{\epsilon_O^2}\frac{g_O^4}{32} + \frac{1}{\epsilon'}\left[K_{Q1}^2 + 6K_{Q2}^2 - \frac{3K_O^2}{2}\right]$$

$$- \frac{1}{\epsilon_Q \epsilon_O}\frac{3g_Q^2 g_O^2}{8} - \frac{1}{(\epsilon_Q + \epsilon_O)}\frac{g_Q^2 g_O^2}{2} + \frac{1}{(\epsilon_Q + \epsilon_O)}\frac{g_Q^2 g_O^2}{2}, \tag{E8}$$

$$Z_f = 1 + \frac{1}{\epsilon_Q}\left[-\frac{g_Q^2}{2} + \frac{g_Q^4}{8}\right] - \frac{1}{\epsilon_Q^2}\frac{g_Q^4}{8} - \frac{1}{\epsilon_O}\frac{g_O^2}{4} + \frac{1}{\epsilon_O^2}\frac{g_O^4}{32} - \frac{1}{\epsilon'}\left[K_{Q1}^2 + 6K_{Q2}^2 + \frac{3K_O^2}{2}\right] + \frac{1}{(\epsilon_Q + \epsilon_O)}\frac{g_Q^2 g_O^2}{2} - \frac{1}{\epsilon_Q \epsilon_O}\frac{3g_Q^2 g_O^2}{8}. \tag{E9}$$

From the renormalization constants, we can compute the beta functions,

$$\frac{dK_i}{d\ln\mu} = K_i\left[\sum_{k=Q_1, Q_2, O} K_k \partial_{K_k} G_{K_i}^{(0,0,1)} + \frac{g_Q}{2}\partial_{g_Q} G_{K_i}^{(1,0,0)} + \frac{g_O}{2}\partial_{g_O} G_{K_i}^{(0,1,0)}\right], \tag{E10}$$

$$\frac{dg_j}{d\ln\mu} = g_j\left[-\frac{\epsilon_j}{2} + \sum_{k=Q_1, Q_2, O} K_k \partial_{K_k} G_{g_j}^{(0,0,1)} + \frac{g_Q}{2}\partial_{g_Q} G_{g_j}^{(1,0,0)} + \frac{g_O}{2}\partial_{g_O} G_{g_j}^{(0,1,0)}\right], \tag{E11}$$

where we Taylor expand the products $Z_f^{-1} Z_{K_i}$ and $Z_f^{-1} Z_{g_j}$ as follows in order to obtain the $G^{(m,n,\ell)}$ factors which appear in Eqs. (E10) and (E11):

$$G_{K_i} \equiv Z_f^{-1} Z_{K_i} = \sum_{m,n,\ell=0}^{\infty} \frac{G_{K_i}^{(m,n,\ell)}(\{K, g\})}{\epsilon_Q^m \epsilon_O^n \epsilon'^\ell}, \tag{E12}$$

$$G_{g_j} \equiv Z_f^{-1} Z_{g_j} = \sum_{m,n,\ell=0}^{\infty} \frac{G_{g_j}^{(m,n,\ell)}(\{K, g\})}{\epsilon_Q^m \epsilon_O^n \epsilon'^\ell}. \tag{E13}$$

The first terms of the series are $G_{K_i}^{(0,0,0)} = G_{g_j}^{(0,0,0)} = 1$, and the indices $i = Q_1, Q_2, O$, $j = Q, O$.

APPENDIX F: EXPONENTS FOR MULTIPOLAR SUSCEPTIBILITY

From the Bose-Kondo beta functions in Eq. (23) and (24) in Sec. III D, the local multipolar moment susceptibilities for the case of zero fixed point values in our model are given by Eq. (28), and turn out to be

$$\gamma_Q = \lambda_O^* + 4((K_{Q1}^*)^2 + 6(K_{Q2}^*)^2 + 3(K_O^*)^2), \tag{F1}$$

if $\lambda_Q^* = 0$, and

$$\gamma_O = 2\lambda_Q^* + 8((K_{Q1}^*)^2 + 6(K_{Q2}^*)^2), \tag{F2}$$

if $\lambda_O^* = 0$. The latter of these two is used to compute the octupolar susceptibility exponent at the critical points $C_{1,2\pm}^Q$.

APPENDIX G: SCALING BEHAVIORS OF MULTIPOLAR SUSCEPTIBILITY AT FINITE TEMPERATURE

The scaling behavior of the multipolar susceptibility as a function of imaginary time in the previous section is for zero temperature. Here, we will discuss how to obtain the scaling behavior for finite temperature. Let us assume that we have conformal invariance at the critical point. Assuming that the multipolar moments are primary operators with conformal

dimension $\gamma_i/2$, the correlation function (susceptibility) of the multipolar moment is [62,82]

$$\langle T_\tau S^i(\tau_1) S^i(\tau_2)\rangle \propto \frac{1}{|\tau_1 - \tau_2|^{\gamma_i}}. \tag{G1}$$

Performing a conformal mapping, $\tau \to f(\tau) = \frac{\pi}{\beta}\tan(\frac{\pi\tau}{\beta})$,

$$\langle T_\tau S^i(\tau_1) S^i(\tau_2)\rangle \to \left(\frac{\partial f(\tau_1)}{\partial \tau_1}\right)^{\gamma_i/2}\left(\frac{\partial f(\tau_2)}{\partial \tau_2}\right)^{\gamma_i/2}$$

$$\times \langle T_\tau S^i(f(\tau_1)) S^i(f(\tau_2))\rangle. \tag{G2}$$

Letting $\tau_1 = \tau$ and $\tau_2 = 0$, then

$$\chi_i(\tau, T) \propto \left(\frac{\pi/\beta}{\sin(\pi\tau/\beta)}\right)^{\gamma_i}. \tag{G3}$$

After Fourier transforming and analytic continuation, we can get the multipolar susceptibility in terms of the temperature T and the energy scaling ω [82,91,92],

$$\chi_i(\omega, T) \propto T^{\gamma_i - 1}\frac{\Gamma(\frac{\gamma_i}{2} - \frac{i\omega}{2\pi T})\Gamma(1 - \gamma_i)}{\Gamma(1 - \frac{\gamma_i}{2} - \frac{i\omega}{2\pi T})}. \tag{G4}$$

The scaling behavior of the real and imaginary parts of $F(\frac{\omega}{T}) \equiv \Gamma(\frac{\gamma_i}{2} - \frac{i\omega}{2\pi T})/\Gamma(1 - \frac{\gamma_i}{2} - \frac{i\omega}{2\pi T})$ is

$$\text{Re}[F(x)] = \begin{cases} F(0) + C_{\text{Re},<}|x|^2, & |x| \ll 1, \\ C_{\text{Re},>}|x|^{\gamma_i - 1}, & |x| \gg 1, \end{cases} \tag{G5}$$

$$\text{Im}[F(x)] = \begin{cases} C_{\text{Im},<}|x|, & |x| \ll 1, \\ C_{\text{Im},>}|x|^{\gamma_i - 1}, & |x| \gg 1, \end{cases} \tag{G6}$$

where $F(0) = \frac{\Gamma(\frac{\gamma_i}{2})\Gamma(1 - \gamma_i)}{\Gamma(1 - \frac{\gamma_i}{2})}$ and $C_{\text{Re},<}$ is a real constant. Then, the temperature dependencies of the real and imaginary parts of the multipolar susceptibility are given in Eqs. (29) and (30), where the constant $C_{\text{Re}1} = C_{\text{Re},<}/F(0)$ in the main text. Note that the real part of the susceptibility exponent at the dc limit ($\omega = 0$) for the Kondo fixed point is consistent with the CFT result [81], $\chi' \sim T^{2\Delta - 1}$, where $\gamma_i = 2\Delta$.

[1] H. Kusunose, J. Phys. Soc. Jpn. **77**, 064710 (2008).

[2] Y. Kuramoto, H. Kusunose, and A. Kiss, J. Phys. Soc. Jpn. **78**, 072001 (2009).

[3] V. Martelli, A. Cai, E. M. Nica, M. Taupin, A. Prokofiev, C. C. Liu, H. H. Lai, R. Yu, K. Ingersent, R. Küchler, A. M. Strydom, D. Geiger, J. Haenel, J. Larrea, Q. Si, and S. Paschen, Proc. Natl. Acad. Sci. USA **116**, 17701 (2019).

[4] E. W. Rosenberg, J. H. Chu, J. P. Ruff, A. T. Hristov, and I. R. Fisher, Proc. Natl. Acad. Sci. USA **116**, 7232 (2019).

[5] B. D. White, J. D. Thompson, and M. B. Maple, Physica C **514**, 246 (2015).

[6] J. Saxena, S. S. Agarwal, P. Ahilan, K. Grosche, F. M. W. Haselwimmer, R. K. Steiner, M. J. Pugh, E. Walker, I. R. Julian, S. R. Monthoux, P. Lonzarich, G. G. Huxley, A. Sheikin, I. Braithwaite, and D. Flouquet, Nature (London) **406**, 587 (2000).

[7] Y. Kohori, Y. Yamato, Y. Iwamoto, and T. Kohara, Eur. Phys. J. B **18**, 601 (2000).

[8] K. Izawa, H. Yamaguchi, Y. Matsuda, H. Shishido, R. Settai, and Y. Onuki, Phys. Rev. Lett. **87**, 057002 (2001).

[9] Y. Aoki, A. Tsuchiya, T. Kanayama, S. R. Saha, H. Sugawara, H. Sato, W. Higemoto, A. Koda, K. Ohishi, K. Nishiyama, and R. Kadono, Phys. Rev. Lett. **91**, 067003 (2003).

[10] E. Bauer, G. Hilscher, H. Michor, C. Paul, E. W. Scheidt, A. Gribanov, Y. Seropegin, H. Noël, M. Sigrist, and P. Rogl, Phys. Rev. Lett. **92**, 027003 (2004).

[11] D. L. Cox, Phys. Rev. Lett. **59**, 1240 (1987).

[12] L. Jiao, Y. Chen, Y. Kohama, D. Graf, E. D. Bauer, J. Singleton, J. X. Zhu, Z. Weng, G. Pang, T. Shang, J. Zhang, H. O. Lee, T. Park, M. Jaime, J. D. Thompson, F. Steglich, Q. Si, and H. Q. Yuan, Proc. Natl. Acad. Sci. USA **112**, 673 (2015).

[13] M. Kratochvílová, J. Prokleška, K. Uhlířová, V. Tkáč, M. Dušek, V. Sechovský, and J. Custers, Sci. Rep. **5**, 15904 (2015).

[14] J. Custers, P. Gegenwart, C. Geibel, F. Steglich, P. Coleman, and S. Paschen, Phys. Rev. Lett. **104**, 186402 (2010).

[15] M. Falkowski and A. M. Strydom, J. Low Temp. Phys. **175**, 498 (2014).

[16] J. Custers, K. A. Lorenzer, M. Müller, A. Prokofiev, A. Sidorenko, H. Winkler, A. M. Strydom, Y. Shimura, T. Sakakibara, R. Yu, Q. Si, and S. Paschen, Nat. Mater. **11**, 189 (2012).

[17] A. S. Cameron, G. Friemel, and D. S. Inosov, Rep. Prog. Phys. **79**, 066502 (2016).

[18] C. Rylands, A. Parhizkar, and V. Galitski, Phys. Rev. B **105**, 195108 (2022).

[19] G. R. Stewart, Rev. Mod. Phys. **73**, 797 (2001).

[20] H. v. Löhneysen, T. Pietrus, G. Portisch, H. G. Schlager, A. Schröder, M. Sieck, and T. Trappmann, Phys. Rev. Lett. **72**, 3262 (1994).

[21] E. Abrahams and P. Wölfle, Proc. Natl. Acad. Sci. USA **109**, 3238 (2012).

[22] V. Y. Irkhin, Eur. Phys. J. B **89**, 117 (2016).

[23] V. Y. Irkhin, Phys. Usp. **60**, 747 (2017).

[24] Y. Iizuka, T. Yamada, K. Hanzawa, and Y. Ōno, in *Proceedings of the International Conference on Strongly Correlated Electron Systems (SCES2019)* (JPS, 2020), https://journals.jps.jp/doi/10.7566/JPSCP.30.011152.

[25] H.-H. Lai, E. M. Nica, W.-J. Hu, S.-S. Gong, S. Paschen, and Q. Si, Kondo destruction and multipolar order–implications for heavy Fermion quantum criticality, arXiv:1807.09258 (2018).

[26] I. Kuzmenko, T. Kuzmenko, Y. Avishai, and G.-B. Jo, Phys. Rev. B **97**, 075124 (2018).

[27] T. Onimaru, K. T. Matsumoto, Y. F. Inoue, K. Umeo, T. Sakakibara, Y. Karaki, M. Kubota, and T. Takabatake, Phys. Rev. Lett. **106**, 177001 (2011).

[28] T. Onimaru and H. Kusunose, J. Phys. Soc. Jpn. **85**, 082002 (2016).

[29] T. Onimaru, K. Izawa, K. T. Matsumoto, T. Yoshida, Y. Machida, T. Ikeura, K. Wakiya, K. Umeo, S. Kittaka, K. Araki, T. Sakakibara, and T. Takabatake, Phys. Rev. B **94**, 075134 (2016).

[30] F. Freyer, J. Attig, S.B. Lee, A. Paramekanti, S. Trebst, and Y. B. Kim, Phys. Rev. B **97**, 115111 (2018).

[31] T. J. Sato, S. Ibuka, Y. Nambu, T. Yamazaki, T. Hong, A. Sakai, and S. Nakatsuji, Phys. Rev. B **86**, 184419 (2012).

[32] K. Araki, Y. Shimura, N. Kase, T. Sakakibara, A. Sakai, and S. Nakatsuji, in *Proceedings of the International Conference on Strongly Correlated Electron Systems (SCES2013)* (JPS, 2013), https://journals.jps.jp/doi/10.7566/JPSCP.3.011093.

[33] M. Matsushita, J. Sakaguchi, Y. Taga, M. Ohya, S. Yoshiuchi, H. Ota, Y. Hirose, K. Enoki, F. Honda, K. Sugiyama, M. Hagiwara, K. Kindo, T. Tanaka, Y. Kubo, T. Takeuchi, R. Settai, and Y. Ōnuki, J. Phys. Soc. Jpn. **80**, 074605 (2011).

[34] K. R. Kumar, H. S. Nair, R. Christian, A. Thamizhavel, and A. M. Strydom, J. Phys.: Condens. Matter **28**, 436002 (2016).

[35] A. Sakai and S. Nakatsuji, J. Phys. Soc. Jpn. **80**, 063701 (2011).

[36] A. Wörl, T. Onimaru, Y. Tokiwa, Y. Yamane, K. T. Matsumoto, T. Takabatake, and P. Gegenwart, Phys. Rev. B **99**, 081117(R) (2019).

[37] K. Matsubayashi, T. Tanaka, A. Sakai, S. Nakatsuji, Y. Kubo, and Y. Uwatoko, Phys. Rev. Lett. **109**, 187004 (2012).

[38] A. Sakai, K. Kuga, and S. Nakatsuji, J. Phys. Soc. Jpn. **81**, 083702 (2012).

[39] M. Tsujimoto, Y. Matsumoto, T. Tomita, A. Sakai, and S. Nakatsuji, Phys. Rev. Lett. **113**, 267001 (2014).

[40] M. Fu, A. Sakai, N. Sogabe, M. Tsujimoto, Y. Matsumoto, and S. Nakatsuji, J. Phys. Soc. Jpn. **89**, 013704 (2020).

[41] T. Onimaru, N. Nagasawa, K. T. Matsumoto, K. Wakiya, K. Umeo, S. Kittaka, T. Sakakibara, Y. Matsushita, and T. Takabatake, Phys. Rev. B **86**, 184426 (2012).

[42] K. T. Matsumoto, T. Onimaru, K. Wakiya, K. Umeo, and T. Takabatake, J. Phys. Soc. Jpn. **84**, 063703 (2015).

[43] T. Onimaru, K. T. Matsumoto, Y. F. Inoue, K. Umeo, Y. Saiga, Y. Matsushita, R. Tamura, K. Nishimoto, I. Ishii, T. Suzuki, and T. Takabatake, J. Phys. Soc. Jpn. **79**, 033704 (2010).

[44] Y. Shimura, M. Tsujimoto, B. Zeng, L. Balicas, A. Sakai, and S. Nakatsuji, Phys. Rev. B **91**, 241102(R) (2015).

[45] S. Nagashima, T. Nishiwaki, A. Otani, M. Sakoda, E. Matsuoka, H. Harima, and H. Sugawara, in *Proceedings of the International Conference on Strongly Correlated Electron Systems (SCES2013)*, Vol. 011019 (Journal of the Physical Society of Japan, 2014), pp. 2–7.

[46] D. J. Schultz, A. S. Patri, and Y. B. Kim, Phys. Rev. Res. **3**, 013189 (2021).

[47] A. S. Patri and Y. B. Kim, Phys. Rev. X **10**, 041021 (2020).

[48] A. S. Patri and Y. B. Kim, SciPost Phys. **12**, 057 (2022).

[49] A. S. Patri, A. Sakai, S.B. Lee, A. Paramekanti, S. Nakatsuji, and Y. B. Kim, Nat. Commun. **10**, 4092 (2019).

[50] A. Tsuruta and K. Miyake, J. Phys. Soc. Jpn. **84**, 114714 (2015).

[51] A. Tsuruta, A. Kobayashi, Y. Ōno, T. Matsuura, and Y. Kuroda, J. Phys. Soc. Jpn. **68**, 2491 (1999).

[52] A. Tsuruta, A. Kobayashi, T. Matsuura, and Y. Kuroda, J. Phys. Soc. Jpn. **69**, 3342 (2000).

[53] A. Tsuruta and K. Miyake, J. Phys. Commun. **6**, 015006 (2022).

[54] A. S. Patri, I. Khait, and Y. B. Kim, Phys. Rev. Res. **2**, 013257 (2020).

[55] S.B. Lee, S. Trebst, Y. B. Kim, and A. Paramekanti, Phys. Rev. B **98**, 134447 (2018).

[56] Q. Si and J. L. Smith, Phys. Rev. Lett. **77**, 3391 (1996).

[57] J. L. Smith and Q. Si, Europhysics Letters (EPL) **45**, 228 (1999).

[58] J. L. Smith and Q. Si, Phys. Rev. B **61**, 5184 (2000).

[59] Q. Si, S. Rabello, K. Ingersent, and J. L. Smith, Nature (London) **413**, 804 (2001).

[60] Q. Si, S. Rabello, K. Ingersent, and J. L. Smith, Phys. Rev. B **68**, 115103 (2003).

[61] A. M. Sengupta, Phys. Rev. B **61**, 4041 (2000).

[62] G. Zaránd and E. Demler, Phys. Rev. B **66**, 024427 (2002).

[63] S. Kirchner, L. Zhu, and Q. Si, Phys. B: Condens. Matter **359-361**, 83 (2005).

[64] L. Zhu and Q. Si, Phys. Rev. B **66**, 024426 (2002).

[65] X. Han and Z. Yu, Phys. Rev. B **104**, 085139 (2021).

[66] F. Steglich, H. Pfau, S. Lausberg, S. Hamann, P. Sun, U. Stockert, M. Brando, S. Friedemann, C. Krellner, C. Geibel, S. Wirth, S. Kirchner, E. Abrahams, and Q. Si, J. Phys. Soc. Jpn. **83**, 061001 (2014).

[67] S. Friedemann, S. Wirth, N. Oeschler, C. Krellner, C. Geibel, F. Steglich, S. MaQuilon, Z. Fisk, S. Paschen, and G. Zwicknagl, Phys. Rev. B **82**, 035103 (2010).

[68] S. Friedemann, N. Oeschler, S. Wirth, C. Krellner, C. Geibel, F. Steglich, S. Paschen, S. Kirchner, and Q. Si, Proc. Natl. Acad. Sci. USA **107**, 14547 (2010).

[69] S. Paschen, T. Lühmann, S. Wirth, P. Gegenwart, O. Trovarelli, C. Geibel, F. Steglich, P. Coleman, and Q. Si, Nature (London) **432**, 881 (2004).

[70] P. Coleman, C. Pépin, Q. Si, and R. Ramazashvili, J. Phys.: Condens. Matter **13**, R723 (2001).

[71] H. v. Löhneysen, A. Rosch, M. Vojta, and P. Wölfle, Rev. Mod. Phys. **79**, 1015 (2007).

[72] M. T. Glossop and K. Ingersent, Phys. Rev. Lett. **99**, 227203 (2007).

[73] J.-X. Zhu, S. Kirchner, R. Bulla, and Q. Si, Phys. Rev. Lett. **99**, 227204 (2007).

[74] Y. Yamane, T. Onimaru, K. Wakiya, K. T. Matsumoto, K. Umeo, and T. Takabatake, Phys. Rev. Lett. **121**, 077206 (2018).

[75] T. Yanagisawa, H. Hidaka, H. Amitsuka, S. Zherlitsyn, J. Wosnitza, Y. Yamane, and T. Onimaru, Phys. Rev. Lett. **123**, 067201 (2019).

[76] T. Yanagisawa, H. Hidaka, H. Amitsuka, S. Zherlitsyn, J. Wosnitza, Y. Yamane, and T. Onimaru, in *Proceedings of J-Physics 2019: International Conference on Multipole Physics and Related Phenomena* (JPS, 2020), https://journals.jps.jp/doi/10.7566/JPSCP.29.015002.

[77] A. A. Abrikosov, Phys. Phys. Fiz. **2**, 5 (1965).

[78] M. A. Ruderman and C. Kittel, Phys. Rev. **96**, 99 (1954).

[79] T. Kasuya, Prog. Theor. Phys. **16**, 45 (1956).

[80] K. Yosida, Phys. Rev. **106**, 893 (1957).

[81] I. Affleck and A. W. W. Ludwig, Phys. Rev. B **48**, 7297 (1993).

[82] M. C. Aronson, M. B. Maple, P. de Sa, A. M. Tsvelik, and R. Osborn, Europhysics Letters (EPL) **40**, 245 (1997).

[83] T. Yanagisawa, S. Mombetsu, H. Hidaka, H. Amitsuka, P. T. Cong, S. Yasin, S. Zherlitsyn, J. Wosnitza, K. Huang, N. Kanchanavatee, M. Janoschek, M. B. Maple, and D. Aoki, Phys. Rev. B **97**, 155137 (2018).

[84] M. E. Sorensen and I. R. Fisher, Phys. Rev. B **103**, 155106 (2021).

[85] A. Tsuruta, A. Kobayashi, T. Matsuura, and Y. Kuroda, J. Phys. Soc. Jpn. **69**, 663 (2000).

[86] S. Nakamura, T. Kano, and S. Ohara, J. Phys. Soc. Jpn. **88**, 5 (2019).

[87] D. J. Schultz, A. S. Patri, and Y. B. Kim, Phys. Rev. B **104**, 125144 (2021).

[88] C.-C. Liu, S. Paschen, and Q. Si, arXiv:2101.01087 (2021).

[89] R. Shiina, O. Sakai, H. Shiba, and P. Thalmeier, J. Phys. Soc. Jpn. **67**, 941 (1998).

[90] R. Shiina, H. Shiba, and P. Thalmeier, J. Phys. Soc. Jpn. **66**, 1741 (1997).

[91] O. Parcollet, A. Georges, G. Kotliar, and A. Sengupta, Phys. Rev. B **58**, 3794 (1998).

[92] O. Parcollet and A. Georges, Phys. Rev. B **59**, 5341 (1999).